JOURNAL OF SPACECRAFT AND ROCKETS
Vol. 35, No. 4, July–August 1998

Semiempirical Method for Predicting Single Event Effect Rates Due to Direct Ionization

Michele M. Gates*
NASA Goddard Space Flight Center, Greenbelt, Maryland 20771
and
Mark J. Lewis†
University of Maryland, College Park, Maryland 20740

A semiempirical method for predicting on-orbit single event effect rates has been developed. The derivation of this technique circumvents the need for assumptions regarding sensitive volume geometry, the use of the concept of effective linear energy transfer, and sensitive volume dimension input. Prediction results are compared to flight data from the Cosmic Ray Upset Experiment, for which the presented method is shown to compare up to an order of magnitude more closely than previous methods when applied both to flight-lot-specific and to generic ground test data. The utility of this method in performing trade studies also is demonstrated through an application of candidate microprocessors.

Nomenclature

E = energy transferred to the medium by ion
F = differential flux of ions (ions/cm^2:time · steradian · MeV) with atomic number Z, mass number A, and energy E
k_t = transport kernel, units area
L = linear energy transfer
x = linear dimension along the ion path length
θ = azimuthal angle
κ = angular incidence factor
σ = error cross section, cm^2
ϕ = polar angle

Introduction

SINGLE event effect (SEE) rate prediction with current industry electronics has become a difficult task. In the space industry, candidate electronic components include commercial devices, for which detailed information about the design and manufacturing process often is not available for use in SEE rate modeling. For these applications, traditional SEE rate prediction methods, which require input of sensitive volume dimensions and assumptions of geometry, may not be ideal. In fact, recently published results have shown that SEE rate predictions can deviate from observed flight SEE rates by orders of magnitude.[1,2] The methodology presented in this work provides rapid SEE rate prediction without the assumptions invoked in traditional SEE rate prediction methods.

In addition, the number of candidate spacecraft devices that are sensitive to SEE continues to increase; therefore, the number of SEE rate predictions required by each space mission is increasing. Where SEE rate prediction previously was performed on the few non-radiation-hardened devices used in a space mission, there currently exists a need for systems-level trade studies to rapidly assess usability of an array of commercial devices in a space radiation environment. To determine the usability of SEE-sensitive devices, the rate of SEE in the mission orbit is compared to the mission requirements.[3] The method enables assessment of candidate device usability by coupling the mission-specific radiation environment with device tolerance as one system for analysis.

Received Aug. 14, 1997; revision received Jan. 4, 1998; accepted for publication Jan. 19, 1998.

*Aerospace Engineer, Advanced Component Technologies.
†Associate Professor, Aerospace Engineering Department.

Methodology

Electronics in orbit are exposed from all directions to the ionizing space radiation environment existing external to the spacecraft, which suggests an integral over the entire device surface to include all impinging particles. The governing equation for SEEs is described by Petersen.[4] The transport-kernel term represents the ability of particle energy deposition and collection phenomena to cause an effect: The transport kernel is equal to one if the deposited charge can cause an effect and equal to zero if the deposited charge cannot cause an effect. The transport kernel and the space particulate environment are integrated over 4π sr to obtain the net effect of an environment incident onto a sensitive geometry from all directions:

$$\text{Rate} = \sum_{\text{Isotopes}} \iiint k_t(Z, A, E, \theta, \phi) \times F(Z, A, E, \theta, \phi)\, \mathrm{d}E \sin\theta\, \mathrm{d}\theta\, \mathrm{d}\phi \tag{1}$$

Several assumptions are employed to simplify Eq. (1) for calculation purposes.[4] It is assumed that the energy deposited into a sensitive volume by an ion is equal to its energy loss as calculated using its impinging linear energy transfer (LET), defined as

$$\text{LET} = \frac{\mathrm{d}E}{\mathrm{d}x} \tag{2}$$

where E is the energy transferred to the medium and x is the linear dimension along the ion path length. In reality, there is some nonlinear motion of a heavy ion, and Xapsos[5] showed that the energy lost by the ion is not exactly equal to the energy deposited into a sensitive volume. It also is assumed that the LET of the incident ion is constant through the sensitive volume, although detailed analysis proves that there is LET variation along the path length.[6] Special precautions, such as the denuding of test devices, are taken in experimental testing to minimize the penetration depth to the sensitive volume.[7] In addition, ions with equal LET values are assumed to produce the same effect on a given sensitive volume, which allows ions to be grouped by LET, a single variable, rather than by atomic number, mass number, and energy. Stapor et al.[8] demonstrated that charge collection by ions of higher energy differs from that by ions of lower energy but equal LET, and they attributed the differences to ion track structures. However, the use of this assumption greatly simpifies the single event upset (SEU) rate prediction. Given these assumptions, the governing equation may be simplified to the form[4]

$$\text{Rate} = \iiint k_t(L, \theta, \phi) F(L, \theta, \phi)\, \mathrm{d}L \sin\theta\, \mathrm{d}\theta\, \mathrm{d}\phi \tag{3}$$

where the LET is represented by L. The behavior of the transport kernel is dependent on the device under consideration. Quantification of a device response with computer solution requires detailed modeling of all internal geometries and materials and functional simulation. Another route is to determine the SEU cross section, the ratio of the number of errors to the test ion fluence, as defined in Eq. (4), through experimental means allowing the replacement of the transport kernel by a variable that is obtainable for practical use[7]:

$$\sigma = \frac{\text{Number of errors}}{\text{Ion fluence}} \tag{4}$$

The space-environment differential flux F is assumed to be omnidirectional and isotropic. The variation in shielding on spherical spacecraft has been found to be relatively ineffective in attenuating heavy ions in the space environment, which are extremely energetic.[9,10] An orbit-averaged flux may be employed to obtain the orbit-averaged SEU rate expected, and a peak flux may be used to obtain the peak flux expected. The resulting expression, which forms the basis of many SEU rate prediction methods, is

$$\text{Rate} = \int\int\int \sigma(L, \theta, \phi) F(L, \theta, \phi)\, \mathrm{d}L \sin\theta\, \mathrm{d}\theta\, \mathrm{d}\phi \tag{5}$$

where σ is the cross section, or the ratio of the cumulative number of errors to the total ion fluence. The proposed method treats error rate prediction by considering the component or device as a single sensitive volume immersed in a particulate environment and by performing a spherical integration, yielding

$$\text{Rate} = \int_0^{2\Pi}\int_0^{\Pi}\int_{L_{\text{th}}}^{L_{\max}} \sigma(L, \theta, \phi) F(L, \theta, \phi)\, \mathrm{d}L \sin\theta\, \mathrm{d}\theta\, \mathrm{d}\phi \tag{6}$$

where the limits of integration are from the threshold LET for the first effect observed, L_{th}, to the maximum LET in the environment considered, $L_{\max}$.

The following assumptions are employed in the proposed method to enable calculation. The cross section σ is assumed to be independent of the polar angle of ion incidence, allowing the device sensitivity $\sigma(L, \theta, \phi)$ to be modeled as $\sigma(L, \theta)$. Recall that the previous methods discuss model device sensitivity as $\sigma(L)$ and employ a model of the sensitive volume. This work utilizes the test data generated directly for azimuthal angles, which replace the effective LET assumption. Device sensitivity also is assumed to be the same for ions entering the device from the front as from the back. Invoking these assumptions yields

$$\text{Rate} = 2\Pi \int_0^{\Pi}\int_{L_{\text{th}}}^{L_{\max}} \sigma(L, \theta) F(L)\, \mathrm{d}L \sin\theta\, \mathrm{d}\theta \tag{7}$$

The integral environment spectra $f(L)$ are obtained from the differential spectra $F(L)$:

$$f(L) = -\int_{L_{\text{th}}}^{\infty} F(L)\, \mathrm{d}L \tag{8}$$

Inserting Eq. (8) into the governing equation results in

$$\text{Rate} = 2\pi \int_0^{\pi}\int_{\infty}^{f_{\text{th}}} \sigma(L, \theta)\, \mathrm{d}f(L) \sin\theta\, \mathrm{d}\theta \tag{9}$$

which represents the heart of this error-rate prediction method.

In the solution procedure described in the following sections, the θ space is discretized into angular sectors defined by the angles used in ion-beam testing. From the interior expression in the equation, in which the cross section is placed in the flux space rather than the LET space, an interesting system is derived for analysis. Here, the device cross section is expressed across an environment flux space, allowing direct assessment of the device in the mission-specific environment.

Experimental angular heavy-ion data typically are interpreted in terms of effective LET and effective cross section, to provide the device response to ions of different LET striking at normal incidence.

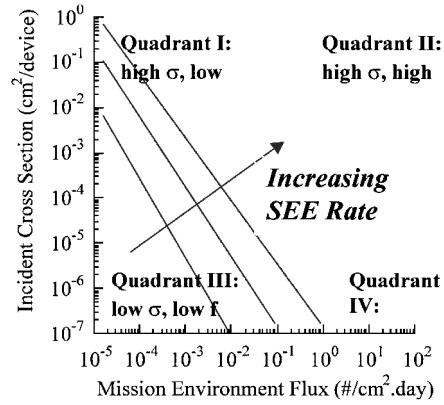

Fig. 1 Generic-device mission system.

However, the experimental data may show scatter beyond experimental error. Research on the effects of ions at different angles of incidence has shown that charge collection is altered significantly with angle of ion incidence, even with the same ion at the same energy, and has been extended to show that cross sections also are affected by angle of ion incidence.[11,12] For test ions of sufficient penetration depth, the angular data obtained in experimentation directly measure edge effects and high-angle impacts, producing cross-section data that inherently include the entire device response. Depending on the facility, these may be only those ions with lower LET; however, ions in the lower LET regime are the most abundant in the space environment and contribute the majority of the SEE rate in devices that are SEE sensitive.[3]

The experimental data provided by the ground facility, effective LET, and cross section were converted to incident LET and cross section using the following equations:

$$\text{LET}_{\text{inc}} = \text{LET}_{\text{effective}} \times \cos(\theta) \tag{10}$$

$$\sigma_{\text{inc}} = \sigma_{\text{effective}} \times \cos(\theta) \tag{11}$$

The interior integral in Eq. (9) suggests the use of omnidirectional environment spectra and incident cross-section data in the same plane. Figure 1 presents the system in generic form, in which device incident cross-section data are graphed with omnidirectional environment integral flux values for corresponding LET. Plotting the device sensitivity as a function of the mission environment flux presents the appropriate question: What is the SEU rate corresponding to this system?

The θ space is discretized in the second step of the solution of Eq. (9). Through the use of the angular incidence factor, the omnidirectional environment is divided into spherical angular sections, $\delta\theta_i = \theta_i$ to θ_{i+1} for $i = 1, \ldots, M$, forming a hemisphere over the top half of the device. The fraction of surface area incident by a specific sector, or angular incidence factor, is derived from spherical coordinates and is given as

$$\kappa = (\cos\theta_1 - \cos\theta_2) \tag{12}$$

where θ_1 is closest to the normal, 0 deg, and θ_2 is the next largest angle sampled, with a maximum of 90 deg. Equation (12) represents the fraction of predicted environment omnidirectional flux incident between angles θ_1 and θ_2 and includes ion incidence onto both the top and the bottom ($+z$ and $-z$) of the device. If the largest angle is less than 90 deg, then an additional segment from the largest angle, θ_1, to 90 deg, θ_2, is added. The use of the device mission system allows the simplification to

$$\text{Rate} = 2\pi \int_0^{\pi}\int_{\infty}^{f_{\text{th}}} \sigma_{\text{inc}}(f, \theta)\, \mathrm{d}f \sin\theta\, \mathrm{d}\theta \tag{13}$$

Here σ_{inc} is the device incident cross section, and f is the predicted omnidirectional integral LET flux for a specific mission orbit profile. The interior integral is accomplished through integration of the device mission system (σ vs f). The range of integration is from the

fluence for LET threshold, f_{th}, of each angular sector to the fluence for the largest LET in the environment prediction, f_{max}.

With the definition of the angular incidence factor, the θ space is discretized into M segments covering $\theta = 0$ to $\pi/2$, and calculations are performed for each $\delta\theta_i$ as

$$\text{Rate}(\delta\theta_i) = \kappa_i \int_{\infty}^{f_{th}} \sigma_{inc}(f)_{i+s}\, df \tag{14}$$

The value of the index s determines which set of cross-section data will be used for each sector. Because device sensitivity varies with angle of ion incidence, for each $\delta\theta_i$ the endpoints θ_i and θ_{i+1} will have different cross sections, σ_i and σ_{i+1}. An upper-bound prediction utilizes the more conservative cross section for each $\delta\theta$, and so it is assumed that the larger of σ_i and σ_{i+1} represents the cross section for the entire sector $\delta\theta_I$. It is often advantageous to have both an upper- and a lower-bound estimate of expected performance for design consideration.

The summation of the SEU rates for each spherical segment yields the predicted SEU rate for the device in the orbital environment as

$$\text{Rate} = \sum_{i=1}^{M} \text{Rate}(\delta\theta_i) \tag{15}$$

Recall that the definition of κ contains a multiplicative factor of 2. Because the device sensitivity is assumed to be hemispherically symmetric, cross-section values obtained experimentally for the top half of the device are applied to the bottom half of the device by scaling the angular incidence factor by 2. The SEU rate is directly proportional to κ and is equivalently scaled. Notice that this solution does not require the explicit modeling of the sensitive volume of the device. Instead, the model uses the sensitive-volume information contained in the angular cross-section data set. Using the incident cross section instead of the effective cross section implicitly models the sensitive volume.

Applications

SEU Rate Analysis of a SRAM (Application 1)

Figure 2 presents a typical heavy-ion ground-test data set, where the x axis presents effective LET of the test ion and the cross section is shown on the y axis.[13] These data were obtained using the standard heavy-ion SEE test method.[7] The data set presented in Fig. 2 represents the SEU sensitivity of a Hitachi 1-Mbit SRAM when the cells are programmed to zero.[13] A data set also exists for the case in which cells are programmed to one but is not shown here.[13]

Note the large variation in cross-section data points for the same effective LET value. In typical SEU rate prediction methods, these data would be curve-fitted to obtain a single effective LET response.[4,14] Figure 3 presents these data transformed to incident LET and cross section, with the angle of test ion incidence

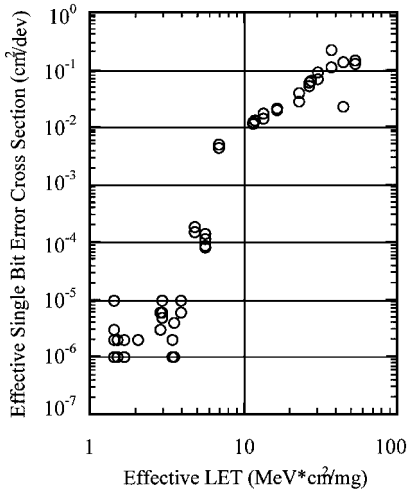

Fig. 2 Hitachi 1-Mbit SRAM ZQ0405 4628128 heavy-ion test data: effective LET vs effective cross section (all cells programmed to 0).

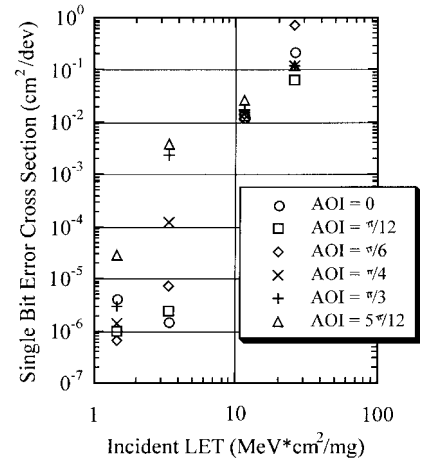

Fig. 3 Hitachi 1-Mbit SRAM heavy-ion test data: incident LET vs cross section.

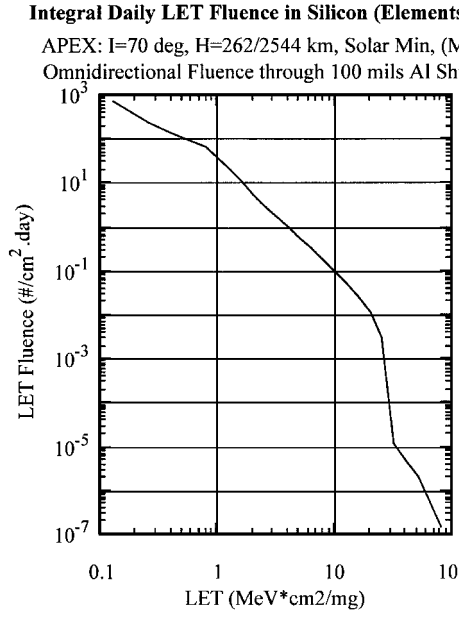

Fig. 4 Heavy-ion LET spectra prediction for APEX spacecraft.

(AOI) shown in the legend. Here it is shown clearly that the device response to angular incident ions is different from that to ions with equal LET at normal incidence. However, because we are not using the effective LET concept, we can see clearly that data scatter at the same incident LET is due to the higher cross section of the device to angular hits.

The predicted mission-specific environment for the Cosmic Ray Upset Experiment (CRUX) on the APEX satellite, on which the Hitachi SRAM flew, was provided by NASA Goddard Space Flight Center Radiation Physics Office and is shown in Fig. 4.

The incident cross-section data are coupled with the mission-specific omnidirectional heavy-ion environment integral LET spectra to produce the device mission system. The plane of incident LET is orthogonal to that presented in the device mission system. Therefore, each point shown on the device mission system has a corresponding incident LET. The device mission system for the Hitachi 1-Mbit SRAMs in the APEX satellite is shown in Fig. 5. Note that, immediately, it can be seen that ions striking at high angles of incidence will cause the highest SEU rate in this orbit. It also is shown graphically in this perspective that ions with LET values to which the SRAM is most sensitive exist in the APEX orbit in far smaller quantities than the quantities of those to which the device is far less sensitive. For this case, the predicted number of particles to which this SRAM is sensitive is about 18, but the number of particles in the APEX orbit that the device is most sensitive to is four orders of magnitude smaller.

Table 1 Hitachi 1-Mbit SRAM on CRUX: prediction results compared to flight data

	SEU rate, E−02 SEUs/device/day		
σ	Lower-bound prediction	On-orbit observations	Upper-bound prediction
1	3.88 ± 0.02	4.40 ± 0.31	5.05 ± 0.24
2	3.88 ± 0.04	4.40 ± 0.62	5.05 ± 0.48
3	3.88 ± 0.06	4.40 ± 0.93	5.05 ± 0.72

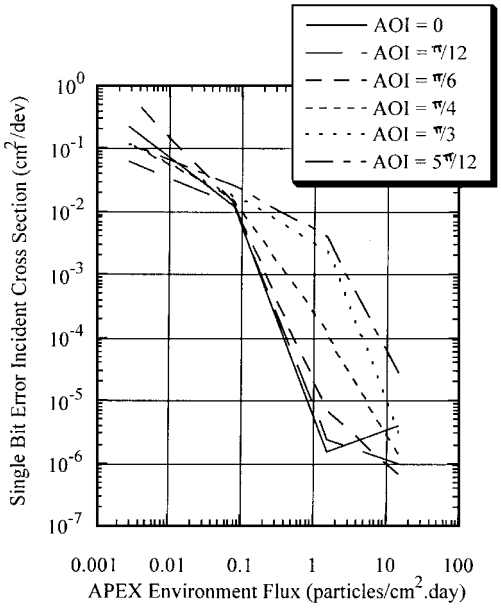

Fig. 5 Device mission system for Hitachi 1-Mbit SRAM in the APEX orbit.

Notice that there exists a complete device mission system for each test ion angle. Because the ground-test data set consisted of data points at specified angles of test ion incidence and the same angles were used for each ion, the test data set created a comprehensive device mission system. The intent is to characterize the entire device, from $\theta = 0$ to $\pi/2$, by defining the sectors to use as much available angular data as possible to approximate the sensitivity of defined adjacent angular sectors.

The device is divided into angular sectors from $\theta = 0$ to $\pi/2$, where the response at each sector's endpoint is defined in the device mission system. The SEU rate for the ith sector is simply the integral under the device mission system curve scaled by κ. Table 1 presents comparisons of the upper- and lower-bound results with published flight data.[1] Because the CRUX mission alternated the programming of all SRAM cells between ones and zeroes every 24 h, the predictions assumed that all cells spent 50% of the time in the zero state and 50% in the one state. Notice the close agreement between the predicted SEU rates and the on-orbit behavior. Variances include uncertainties in the measurement of cross section, as calculated from the experimental data sets.

To bound the SEU rate, an upper-bound prediction was obtained using the highest of the two endpoint cross sections to represent each sector's sensitivity. A lower-bound prediction utilized the lowest of the two cross sections of each angular sector to represent the sensitivity of the sector.

Use of Generic Test Data (Application 2)

Other than the data used for the prediction presented in application 1, only generic ground-test data or test data on the same device type from a different lot were available for the SRAMs on the CRUX experiment. In fact, all previously reported SEU rate predictions performed for the CRUX SRAMs used generic ground-test data.[2] The use of generic test data is common in SEU rate prediction because of the rarity of having lot-specific ground-test data for the mission under consideration. This section presents the application of the proposed method to SEU rate prediction using generic ground-test data. SEU rate predictions were performed for three SRAM types on CRUX: the Hitachi 1-Mbit SRAM HM658128, the Micron 1-Mbit SRAM MT5C1008C-25, and the Micron 256-Kbit SRAM MT5C2568. Results are compared to on-orbit observations, consisting of daily average SEU rates and standard deviation data on the 16 to 40 samples for each of the three SRAMs.[2] Comparisons also are performed with other reported predictions that used the same input data sets of test data and environment spectra.[1,2,13,15]

Figure 6 presents data for the Hitachi 1-Mbit SRAM HM658128, the Micron 1-Mbit SRAM MT5C1008C-25, and the Micron 256-Kbit SRAM MT5C2568 extracted from generic ground-test data sets.[13,15] The Hitachi 1-Mbit SRAM has the lowest cross section of the three, with the Micron 256-Kbit being the highest, except at high LET. Test data were implemented in which the angle of test ion incidence was 0 deg because the experiments were not performed at specific angles. The device mission system for the three SRAMs in the APEX environment was calculated and is presented in Fig. 7. The APEX mission heavy-ion flux is shown on the x axis, and the generic device sensitivity data are on the y axis. The Hitachi 1-Mbit SRAM should have the lowest SEU rate in this mission. The Micron 256-Kbit and 1-Mbit SRAMs look as if the SEU rates will be about equal in this mission. Note that qualitative SEU rate comparison is not evident solely from examination of Fig. 6. This is particularly important in system engineering trade studies, where comparison between devices is important.

SEU rates were calculated using the proposed method with the generic test data sets. The cross section for 0 deg was assumed to be representative of the entire angular sector 0 to $\pi/2$. Hence, $\kappa = 1$ for

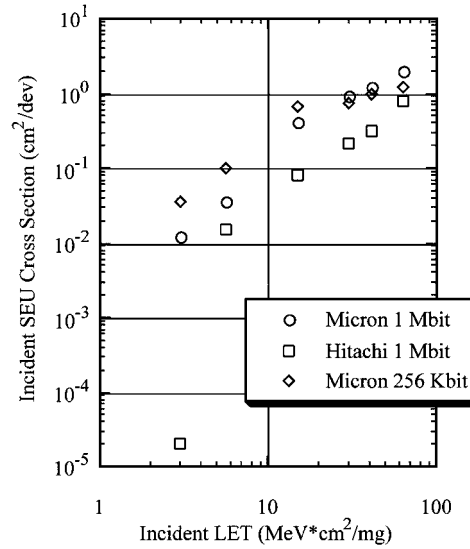

Fig. 6 Generic ground-test heavy-ion data for SRAMs on the CRUX Experiment.

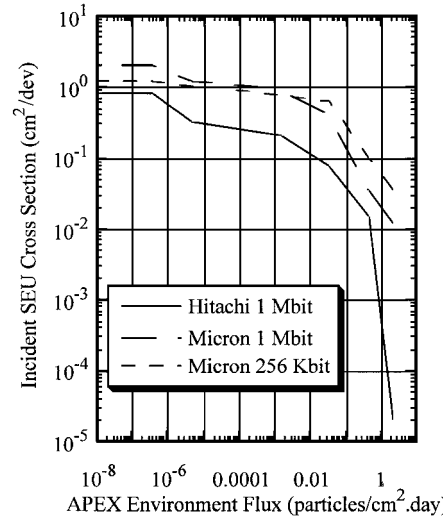

Fig. 7 Device mission system for SRAMs on the CRUX Experiment using generic ground-test data.

Table 2 Generic SRAMs on CRUX: prediction results compared to flight data

SEU rate source	SEUs/device/day		
	Hitachi 1-Mbit	Micron 1-Mbit	Micron 256-Kbit
On-orbit observations	(4.40 ± 0.31)E−02	(22.0 ± 11.0)E−02	(25.5 ± 2.8)E−02
Semiempirical method	3.88E−02	15.8E−02	30.1E−02
CREME prediction	8.40E−02	89.4E−02	249E−02
Integral Weighting prediction	6.45E−02	68.5E−02	164E−02
Figure-of-Merit prediction	5.73E−02	26.2E−02	83.7E−02
NOVICE prediction	2.05E−02	23.4E−02	184E−02

all of these predictions. For this simplified prediction, each device SEU rate is equal to the area under each curve. Table 2 presents results of SEU rate predictions performed using the proposed method, again using the daily-average environment for 176 days. Note that the predicted SEU rate for the Micron 256-Kbit SRAM is the highest of the three and that the Hitachi 1-Mbit SRAM was predicted to have the lowest SEU sensitivity in the APEX orbit. This relative comparison agrees with results of analysis of the device mission system.

The closest comparison of this semiempirical method with the flight results was for the Hitachi 1-Mbit SRAM, where the prediction is 12% less than the observed value. The Figure of Merit was the second closest, where the prediction was 30% higher than the flight observation. The CREME prediction was the least accurate, with an error of a factor of 2. Because the observed flight data measurements have a low standard deviation and the input into all predictions was the same, differences between the SEU rate predictions and the flight observations are due to the different prediction methods.

The largest difference between the results from proposed method and flight observations were found for the Micron 1-Mbit SRAM, for which the calculation of SEU rate was 28% lower than the observed value. This semiempirical method proved more accurate than both the Integral Weighting and CREME predictions, which were a factor of two and three too large, respectively. Here the NOVICE and Figure of Merit results were 6% and 19% greater than the flight observations, respectively. Notice also that the result of the generic SEU rate prediction for the Hitachi SRAM is slightly lower than the lower-bound lot-specific prediction shown in Table 1. This is consistent with the methodology in the prediction procedure presented; because the lower-bound lot-specific prediction assumed each angular sector sensitivity to be represented by the smaller cross section, the use of only one angular sector is truly the lowest-bound estimate for this device. The large standard deviation in the observed flight data for the 23 Micron 1-Mbit SRAMs, equal to 52%, probably contains lot-to-lot variance, though special action was taken to procure from only one lot.[2]

Table 2 also presents the comparison of results from this semiempirical method for the Micron 256-Kbit SRAM with reported flight data and other prediction methods.[1] Here we can see that the proposed semiempirical SEU rate prediction result was 18% higher than the observed flight data. All of the other methods overpredicted the SEU rate. The CREME prediction was an order of magnitude higher than the flight data, which is over 70 standard deviations. The Integral Weighting and NOVICE predictions are factors of 6 and 7, respectively, greater than the flight data. With the reasonable variance in the flight observation data for this device—less than 11% of the reported result[1]—it can be concluded that the method presented in this work is clearly the most accurate for this case. Note that the SEU rate for the Hitachi 256-Kbit device is higher than that for the Hitachi 1-Mbit device. These results are in contrast to the common perception that, as a technology matures, it becomes more SEU sensitive. Although it often is assumed that design changes, manufacturing revisions, and technology improvements will increase device sensitivity, the opposite is sometimes the case, as is shown here. These unexpected results emphasize the advantage of the proposed method because it requires no assumptions or input regarding device internals or sensitive volumes.

Microprocessor Trade Study (Application 3)

This section presents the utility of the device mission system in trade-study analysis. The mission scenario presented for this application includes the comparison of the SEU rates of several commercial microprocessors for the MAP mission, located at L2, which is essentially in free space, or geomagnetically unshielded. Available SEU ground-test data for each candidate microprocessor were obtained.[16] Because of the variety of test angles used, only data points for 0-deg angle of ion incidence, or normal incidence, were selected for use and transformed to incident LET. The free-space integral LET spectra were obtained from analyses performed for the MAP mission project office. The device mission system for the microprocessors in the MAP orbital environment was produced by graphing the ground-test incident cross-section data with MAP mission omnidirectional fluences for corresponding incident LET and is shown in Fig. 8.

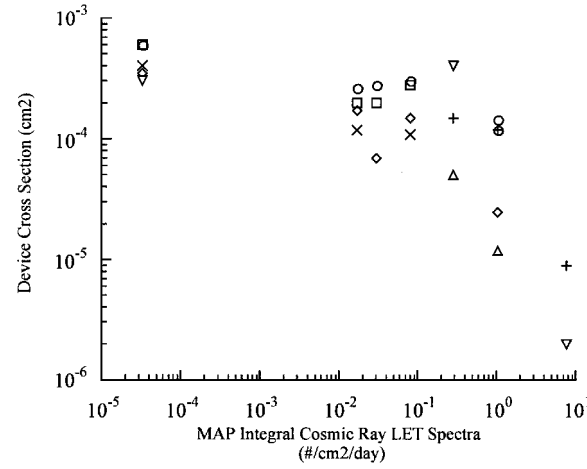

Fig. 8 Device mission system for candidate microprocessors for the MAP spacecraft. MAP commercial microprocessor trade study. Orbit = L2; 50 mils solid Al spherical shielding: ○, 486DX2-66 cache-on SEU; □, 486DX2-66 cache-on lockup; ◇, 486DX2-66 cache-off SEU; ×, 486DX2-66 cache-off lockup; +, 486DX-33 cache-on; △, 486DX-33 cache-off; and ▽, 80386-20/B.

Different types of SEU were observed in the microprocessors during heavy-ion testing, and cross sections were determined for each type. The data points designated as SEU represent transient errors detected in output of the processor. The lockup data points refer to a test mode that the device entered and from which reset was necessary to restore normal functionality.[16] These two types of SEUs have far different system impacts, and although they are shown on the same device mission system, the failure modes are distinguished in the analysis. In addition, the SEU test results showed different sensitivity to SEU, depending on whether the cache memory was used; therefore cross-section data are presented for each case.[16]

Notice the data points that fall in the top right region of the system, including the 80386-20/B SEU, the 486DX2-66 SEU for cache-on mode, and the 486DX-33 SEU for cache-on mode. This device should experience the highest SEU rates of the group, based on this brief examination. Note that the data points for the 486DX-33 device do not extend beyond a MAP flux of about 0.1 particles/cm^2 · day. This device displayed destructive latchup at an LET of about 20 Me V · cm^2/mg; therefore, SEU data for higher LET values do not exist.

Because all of these data are representative of 0-deg angle of ion incidence, κ is equal to 1, and the SEU rate of each data set is simply the integral under each curve. The calculation was performed for each using the trapezoidal rule and is shown in Table 3. The highest SEU rate predicted was the 80386/20-B, with one SEU or

Table 3 SEU rate predictions: candidate microprocessors for MAP mission

Microprocessor	SEE type	MTBF[a] (years) = 1/SEU rate
486DX2-66 cache-on	SEU	<24
486DX2-66 cache-on	SEFI	40
486DX2-66 cache-off	SEU	<55
486DX2-66 cache-off	SEFI	90
486DX-33 cache-on and cache-off	Destructive latchup	N/A
386-20/B	SEU also nondestructive microlatchup	<25
Mongoose 1	SEU	2.9E+04
Honeywell SOI test metal	SEU	1E+14

[a]Mean time before failure.

lockup expected every 1.7 years. The 486DX2-66 was predicted to experience an upset every 11.6 years with cache on. The SEU rate for the 486DX-33 was not obtainable because the device experienced destructive latchup at LET = 20 MeV · cm^2/mg. Notice that these findings are similar to those found upon quantitative examination of the device mission system. The predicted SEU rate for the 486DX2-66 when cache is not used was considerably less than that of the other candidates. In cache-off mode, the predicted SEU was once every 37 years. Also note that the predicted rate of lockup was much less than that of SEU. The determination of different cross sections for these failure modes was extremely helpful in this analysis.

Conclusions

The semiempirical method developed in this work enables rapid SEU rate prediction, which is shown to be more accurate when applied to devices that are sensitive to SEU, or have low LET threshold. The methodology is shown to circumvent inputs and assumptions regarding sensitive-volume geometry or dimensions and does not employ the effective LET approximation. Thus, this method does not introduce the errors associated with such assumptions. Results compare the method proposed with other available error-rate prediction methods and with daily average flight data from the CRUX experiment on the APEX mission, which represents an average over approximately 176 days. All predictions were performed using the same input test data and environment models. The environment model was selected to simulate the orbital environment during the flight data collection, providing daily fluxes for a quiet environment during solar minimum, because the APEX environment has remained approximately static during data collection. Holding the environment model and ground-test data sets as constants in the comparisons has allowed the results shown to establish the increased accuracy of this method over other methods in modeling the error rate of devices that are sensitive to SEE. A trade study also is presented to demonstrate the system-level capability of this methodology. The application of such analyses in early design stages is critical to maintaining the shortened schedules in today's industry. Note that this method applies only to events induced by direct ionization. The analysis of events due to indirect ionization is not covered in this work.

Acknowledgments

The authors would like to express their gratitude to several individuals who have enabled this work, specifically, Janet Barth, for kindly providing environment data critical to this work, such as that shown in Fig. 4; Ann Garrison-Darrin, for her tremendous leadership and empowering environment; Henning Leidecker, for invaluable insight and technical interchange; and Kenneth LaBel, for the professional opportunity and support to pursue this work.

References

[1]Adolphsen, J., Barth, J. L., Stassinopoulos, E. G., Gruner, T., Wennersten, M., LaBel, K. A., and Seidleck, C. M., "SEE Data from the APEX Cosmic Ray Upset Experiment: Predicting the Performance of Commercial Devices in Space," *Proceedings of the Third European Conference on Radiation and Its Effects on Components and Systems* (Arcachon, France), RADECS, 1995, pp. 572–580.

[2]Adolphsen, J., Barth, J. L., Stassinopoulos, E. G., Gruner, T., Wennersten, M., LaBel, K. A., and Seidleck, C. M., "Single Event Upset Rates on 1 Mbit and 256 Kbit Memories: CRUX Experiment on APEX," *IEEE Transactions on Nuclear Science*, Vol. 42, No. 6, 1995, pp. 1964–1974.

[3]Gates, M. M., Barth, J. L., Stassinopoulos, E. G., Johnston, A., LaBel, K. A., and Marshall, P., "Single Event Effect Criticality Analysis," NASA HQ Code QW Document, Feb. 1996.

[4]Petersen, E. L., Pickel, J. C., Adams, J. H., Jr., and Smith, E. C., "Rate Prediction for Single Event Effects—A Critique," *IEEE Transactions on Nuclear Science*, Vol. 39, No. 6, 1992, pp. 1577–1599.

[5]Xapsos, M. A., "Applicability of LET to Single Events in Microelectronic Structures," *IEEE Transactions on Nuclear Science*, Vol. 39, No. 6, 1992, pp. 1613–1621.

[6]Jordan, T. M., and Stassinopoulos, E. G., "Variations of Heavy Ion Energy and Linear Energy Transfer (LET) with Penetration in Silicon," NASA Reference Publication 1259, 1991.

[7]"Standard Guide for the Measurement of Single Event Phenomena from Heavy Ion Irradiation of Semiconductor Devices," American Society for Testing and Materials, F1192-88, Dec. 1988.

[8]Stapor, W. J., McDonald, P. T., Knudson, A. R., Campbell, A. B., and Glagola, B. G., "Charge Collection in Silicon for Ions of Different Energy but Same Linear Energy Transfer (LET)," *IEEE Transactions on Nuclear Science*, Vol. 35, No. 6, 1988, pp. 1585–1589.

[9]Massengill, L. W., "SEU Modeling and Prediction Techniques," *Proceedings of the IEEE Nuclear and Space Radiation Effects Conference Short Course*, IEEE Publishing Services, Piscataway, NJ, 1993, pp. 15–26.

[10]"Far Ultraviolet Spectroscopic Explorer Mission Requirements Document," NASA Document GSFC-410-FUSE-002, June 1994, p. 25.

[11]McNulty, P. J., Beauvais, W. J., Reed, R. A., Roth, D. R., Stassinopoulos, E. G., and Brucker, G. J., "Charge Collection at Large Angles of Incidence," *IEEE Transactions on Nuclear Science*, Vol. 39, No. 6, 1992, pp. 1622–1629.

[12]Reed, R. A., McNulty, P. J., and Abdel-Kader, W. G., "Implications of Angle of Incidence in SEU Testing of Modern Circuits," *IEEE Transactions on Nuclear Science*, Vol. 41, No. 6, 1994, pp. 2049–2054.

[13]Moran, A. K., "Single Event Effect Test Report for GSFC Trip to BNL March 27–29, 1996, Version 1.0," Office of Flight Assurance Information Center, Code 300, NASA Goddard Space Flight Center, Greenbelt, MD, April 1996.

[14]Normand, E., "Single Event Effects in Systems Using Commercial Electronics in Harsh Environments," *Proceedings of the 1994 IEEE Nuclear and Space Radiation Effects Conference Short Course*, IEEE Publishing Services, Piscataway, NJ, 1994, pp. V-51–V54.

[15]Koga, R., Crain, W. R., Crawford, K. B., Lau, D. D., Pinkerton, S. D., Yi, B. K., and Chitty, R., "On the Suitability of Non-Hardened High Density SRAMs for Space Applications," *IEEE Transactions on Nuclear Science*, Vol. 38, No. 6, 1991, pp. 1507–1513.

[16]Moran, A. K., LaBel, K. A., Gates, M. M., Seidleck, C. M., McGraw, R., Broida, M., Firer, J., and Sprehn, S., "Single Event Effect Testing of the Intel 80386 Family and the 80486 Microprocessor," *Proceedings of the Third European Conference on Radiation and Its Effects on Components and Systems* (Arcachon, France), RADECS, 1995, pp. 263–269.

A. C. Tribble
Associate Editor